

# IMAGING SPECTROSCOPY APPLIED TO MINERAL MAPPING OVER LARGE AREAS: IMPACT OF RESIDUAL ATMOSPHERIC ARTEFACTS IN REFLECTANCE SPECTRA ON MINERAL IDENTIFICATION AND MAPPING

*Raymond F. Kokaly<sup>1</sup>, Gregg A. Swayze<sup>1</sup>, K. Eric Livo<sup>1</sup>, Todd M. Hoefen<sup>1</sup>, Bernard E. Hubbard<sup>2</sup>, John M. Meyer<sup>3</sup>, Evan M. Cox<sup>1</sup>, Will R. Gnesda<sup>1</sup>*

<sup>1</sup>U.S. Geological Survey, Denver, Colorado, USA

<sup>2</sup>U.S. Geological Survey, Reston, Virginia, USA

<sup>3</sup>Colorado School of Mines, Golden, Colorado, USA

## ABSTRACT

Around the world, imaging spectroscopy (hyperspectral imaging) has been successfully applied to mapping surface minerals over small areas. In this paper, we examine one challenge to reliably mapping surface mineral composition over large areas: the impacts of atmospheric artefacts in reflectance spectra on mineral identification. To examine these impacts, we use a set of Airborne Visible and Infrared Imaging Spectrometer-Classic (AVIRISc) data collected over ~30,000 sq. km of southern California (SoCal) in 2018. The AVIRISc2018 SoCal reflectance data showed residual atmospheric contamination in wavelength regions at the edges of strong water vapor absorption features: 1.44–1.5  $\mu\text{m}$ , 1.75–1.8  $\mu\text{m}$ , and 2.35–2.5  $\mu\text{m}$ . These three regions of atmospheric residuals affect identification and discrimination of mineral absorption features, especially when mineral abundances are low and spectral features are weak. Of these three regions, improving atmospheric correction of imaging spectrometer data in the 2.35–2.5  $\mu\text{m}$  region will result in the most enhancement in mineral identification, discrimination, and mapping. An additional region near 2.2  $\mu\text{m}$  affects phyllosilicate mineral identification. The cause of the distorted reflectance in this region is still being investigated.

**Index Terms**— Hyperspectral, mineral mapping, geology, spectral feature comparison, PRISM/MICA.

## 1. INTRODUCTION

Imaging spectroscopy (hyperspectral imaging) in the visible to shortwave infrared (VSWIR) has been applied to mapping of surface mineral compositions for site specific studies for more than 20 years. To date, we have few examples of using imaging spectrometer data over large areas, considered here as the coverage of a Landsat scene (~34,000 sq. km); one such example is the U.S. Geological Survey (USGS) mineral map of Afghanistan [1]. National space and science agencies are increasing their use of hyperspectral technology, including the launch of imaging spectrometers to collect narrow swath data (e.g., DESIS,

DLR Earth Sensing Imaging Spectrometer; HISUI, Hyperspectral Imager Suite), and planned missions for narrow swath/limited collection spaceborne sensors (EMIT, Earth Surface Mineral Dust Source Investigation; EnMap, Environmental Mapping and Analysis Program). Furthermore, several space agencies are planning to collect global coverage of imaging spectrometer data, including the Surface Biology and Geology (SBG) study by the National Aeronautics and Space Administration (NASA), and the Copernicus Hyperspectral Imaging Mission for the Environment (CHIME) of the European Space Agency. Clearly, greater attention needs to be given to the challenges posed to generating maps over large areas with imaging spectrometer data. In this paper, we examine one such challenge: the impacts of atmospheric artefacts in reflectance spectra on mineral identification and mapping.

## 2. AVIRIS-CLASSIC 2018 DATA

AVIRISc imaging spectrometer data for CA and NV in 2018 were obtained from the NASA/Jet Propulsion Laboratory (JPL) archive (<https://aviris.jpl.nasa.gov/>). These data, consisting of 176 flight lines, cover approximately two-thirds of CA and one-third of NV (~380,000 sq. km) with ~15 m ground sampling distance. These data were collected on 22 days distributed over the months of January, May-June, and August-September. Because there is redundancy (repeat coverage) among the 2018 AVRIS flight lines, our work to date has focused on a subset of ~80 flight lines. This paper focuses on preliminary reflectance spectra and mineral mapping results for 10 flight lines in the southern California (SoCal) region (Fig. 1).

## 3. ATMOSPHERIC CORRECTION AND CONVERSION TO REFLECTANCE

We applied a radiative transfer (RT) atmospheric correction algorithm to the AVIRISc2018 radiance data to convert to apparent surface reflectance, specifically, the ATCOR4 rugged terrain model [2]. The resulting apparent surface reflectance data are referred to herein as “RT-only” data.

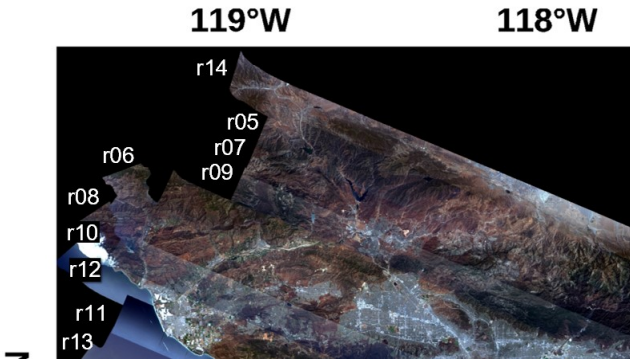


Figure 1. Focal area of S. California AVIRISc2018 flight lines.

The rugged terrain module was used with a 10 m digital elevation model. For each pixel of AVIRISc data, the ATCOR4 model derived slope and aspect to correct for illumination variations. The 820 nm water vapor feature was used for pixel-by-pixel correction of atmospheric water vapor. The rural aerosol model was used for estimation of atmospheric scattering with 120 km specified as the visibility. The SPECTRAL\_CAL function of ATCOR4 was not applied to the AVIRISc data, with the assumption made that the AVIRISc calibration done by NASA/JPL was valid. The ranges of surface and atmospheric factors affecting reflectance within the AVIRISc2018 SoCal coverage, such as surface elevation and aerosol type, are greater than the distribution of in situ data sources, for example, only three Aeronet (Aerosol Robotic Network) sites fall within the coverage. However, other data in the larger CA/NV AVIRISc2018 coverage include both Aeronet and RadCalNet sites that could either be incorporated into the atmospheric correction procedure or used as validation data.

Next, a modification of the ground calibration method of Clark et al. [3] was applied to the RT-only data using field-measured reflectance of a reference site; the resulting data are referred to herein as radiative transfer ground calibrated (RTGC). Because a spectral anomaly was observed between adjacent RTGC flight lines, a modification of the cross-calibration method of Kokaly et al. [1] was applied. We used sparsely vegetated areas of overlap between the ground-calibrated flight line (r08) and adjacent flight lines (r06 to the north and r10 to the south) to compute cross-calibration factors. The resulting data from cross calibration are referred to as CCRTGC data. The multiplier correction factor for cross calibration was computed as the average ratio of spectra in overlap areas between the ground-calibrated flight line to the adjacent indirectly calibrated flight line (mCCRTGC), for example,  $m_{CCRTGC} = RTGC_{r08}/RTGC_{r06}$ , averaged for five overlap areas.

The cross calibration was extended to additional flight lines using the overlap between each flight line (e.g., applying  $CCRTGC_{r06}$  to cross calibrate the adjacent flight line  $RTGC_{r09}$ ). Note that the flight lines are numbered in

order of acquisition (time sequenced); thus, adjacent flight lines may not be numbered in spatial sequence (see Fig. 1 for numbering). The ground-calibrated flight line r08 is one of the central lines. Iteratively, all other flight lines towards the periphery were cross calibrated, successively using overlapping, unvegetated areas.

#### 4. EVALUATION OF REFLECTANCE SPECTRA

Field spectra were measured using an Analytical Spectral Devices (ASD) field spectrometer in 2013, 2014, and 2015. The field spectra were collected along traverses that ranged in length from 30 to 390 m. For each traverse, ASD spectra were averaged and convolved to spectral characteristics of AVIRISc2018. The corresponding pixels of the image data were averaged and compared to visually assess the wavelength regions in AVIRISc2018 data that exhibit residual atmospheric artefacts, for example, Figure 2.

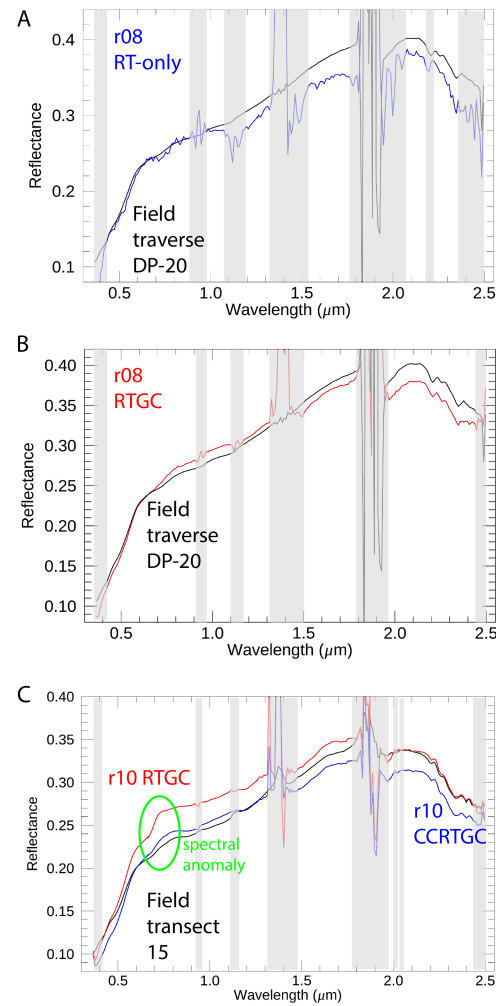


Figure 2. Reflectance spectra from AVIRISc2018 images compared to field data for A) flight line r08 RT-only data, B) flight line r08 RTGC data, and C) flight line R10 RTGC and CCRTGC data. NOTE: areas of poor comparison between image and field

data because of atmospheric residuals or other factors are shown in the gray shading.

Large residual artefacts are present in RT-only data compared to the field data in the water vapor absorption regions around 1.2, 1.4, and 1.9  $\mu\text{m}$  (Fig. 2A). The residuals are greatly reduced in the RTGC data compared to field data, at least for this ground-calibrated flight line (run08) (Fig. 2B). Additionally, the RTGC spectrum has greater similarity in spectral shape to the field data than the RT-only data in the wavelengths longer than 2.35 mm. The comparison of the RTGC data of the adjacent flight line (run10) to the field data revealed an artefact in the near-infrared (NIR) portion of the AVIRISc2018 wavelength coverage (circled region in Fig. 2C). This artefact motivated the CCRTGC step. The CCRTGC spectrum (blue line) has greater correspondence to the field data (black line) than the RTGC data (red line) (Fig. 2C). However, the three reflectance datasets all have residual atmospheric artefacts as illustrated with gray-shaded areas (Fig.2).

## 5. MINERAL MAPPING

We used the Material Identification and Characterization Algorithm (MICA) spectral feature comparison method to create mineral maps. This method, as described in Graham et al. [4], was adapted from HyMap to AVIRIS to map a suite of minerals with diagnostic absorption features in the shortwave infrared (SWIR) wavelength range. In this paper, we focus on only the mineral mapping with the SWIR and not the visible/NIR (VNIR) range. MICA identifies the spectrally dominant mineral(s) in each pixel of an image cube by comparing continuum-removed spectral features in its reflectance spectrum to continuum-removed absorption features in reference spectra of minerals, vegetation, water, and other materials.

MICA was applied for mineral mapping to an AVIRISc flight line subject to the RT-only, RTGC, and CCRTG correction methods. An example comparison of RT-only and RTGC results are shown in Figure 3. As a result of the spectral distortions noted in the previous section of this paper, we see noticeably fewer minerals are detected in the maps of AVIRIS data of RT-only data (Fig. 3A), as compared to the RTGC data (Fig. 3B). Notably, epidote/chlorite, gypsum, and mixtures of white mica and other minerals are either not detected in the RT-only data, or their detections are limited in extent. Where minerals are detected in the RT-only data, the mineral absorption features are very deep, that is, detections are restricted to where these minerals are relatively abundant. For example, areas of abundant kaolinite and calcite are consistent between the atmospheric correction methods. Comparing the mineral distributions (Fig.3), however, more minerals can clearly be mapped in a greater number of pixels using ground-calibrated reflectance data.

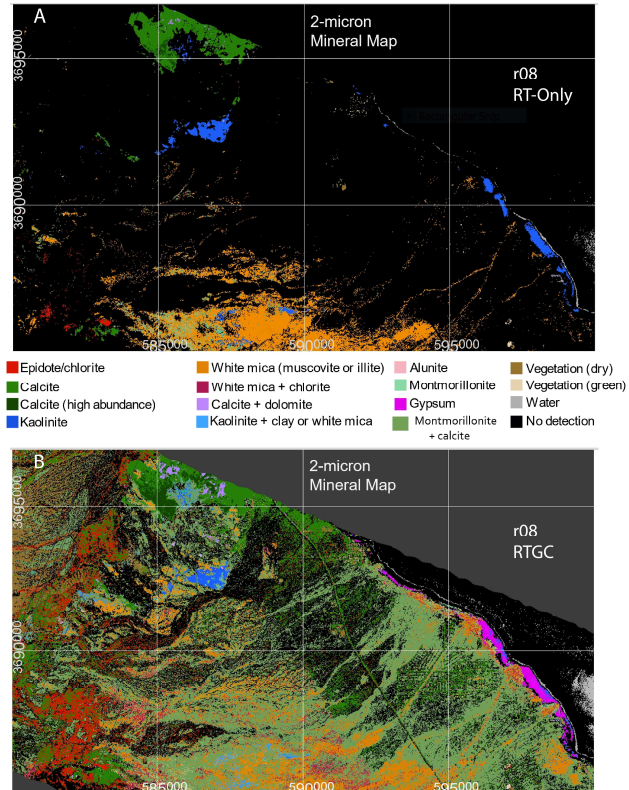


Figure 3. Mineral maps produced using the MICA 2-micron command file for a portion of flight line r08 of AVIRISc2018 data: A) RT-only data, and B) RTGC data. Map projection is UTM zone 11 with datum WGS-84. Map grid lines are at 5 km intervals. Pixel spacing is 15 m.

## 6. DISCUSSION: IMPACT OF RESIDUAL ATMOSPHERIC ARTEFACTS ON MINERAL IDENTIFICATION AND MAPPING

Based on preliminary results for the AVIRISc2018 data over SoCal, we saw the MICA spectral feature comparison method to map minerals was strongly affected by the residual errors in reflectance found in the RT-only data. To a lesser extent, RTGC and CCRTGC data are affected by atmospheric residuals. We evaluated the reference spectra and spectral features listed in the MICA command file for their sensitivity to the affected wavelength regions. Wavelength region usage in the MICA 2-micron mineral mapping is plotted in Figure 4, with the y-axis showing the number of times a channel/wavelength is used to identify a material/mineral. Gray-shaded areas in Fig. 4 indicate wavelength regions of residual atmospheric artefacts seen in the visual comparison of RT-only and CCRTGC data to field-measured reflectance (see Fig. 2).

In the plot for RT-only data (Fig. 4A), we see that the greatest channel usage in the wavelength regions affected by residual atmospheric artefacts is for a small region around 2.2  $\mu\text{m}$  and a larger region ~2.35 to 2.5  $\mu\text{m}$ . The artefact in the 2.2  $\mu\text{m}$  region of RT-only data is being investigated,

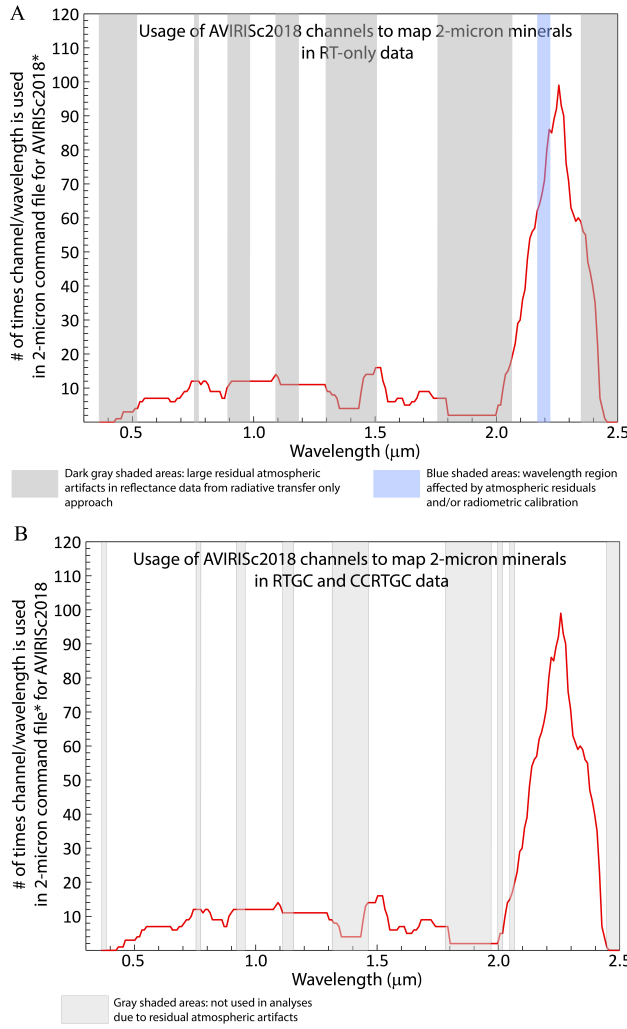


Figure 4. Channel usage in the MICA 2-micron command file (version 2b with 87 entries, of which 72 were mineral entries) applied to AVIRISc2018 data for A) RT-only, and B) RTGC and CCRTGC data. Shaded areas indicating areas of residual atmospheric contamination, appropriate for each data type (see the spectra in Fig. 2).

with the potential source of the artefact being the sensor's radiometric calibration and/or an atmospheric-correction related residual from a weak water vapor absorption in that wavelength region. Significantly, a wide wavelength region is affected by atmospheric residuals and low sensor signal-to-noise ratio at the longward end of the VSWIR wavelengths,  $\sim 2.35$  to  $2.5 \mu\text{m}$ . Because their primary absorption features are centered within the  $2.32$  to  $2.36 \mu\text{m}$  range, this wavelength region is used extensively to identify and discriminate carbonates, amphiboles, serpentines, chlorites/epidote, and talc. Furthermore, some of these minerals have secondary absorption features centered at even longer wavelengths,  $2.38$  to  $2.4 \mu\text{m}$ . In addition, the white mica (muscovite and illite) has secondary absorption features centered around  $2.35 \mu\text{m}$ , which are used to differentiate them from montmorillonite.

Given the same command file, channel usage for mineral mapping with RTGC or CCRTGC data is the same as for RT-only data; however, the wavelength regions affected by atmospheric residuals are minimized for RTGC and CCRTGC data compared to RT-only data (compare the shaded areas in Fig. 4. The effect of the ground calibration and cross calibration is to lessen the extent of wavelength regions in reflectance data that are affected by residual atmospheric contamination. Because the MICA 2-micron command file is based on 20 years of analyzing airborne imaging spectrometer data, we see that the gray areas in Figure 4B often correspond with drops in channel usage. This is a result of the MICA 2-micron command file being written to avoid analyzing spectral features within the wavelength regions that are strongly affected by the atmosphere.

Advances in RT-only atmospheric correction methods that increase quality in the  $2.35$  to  $2.5 \mu\text{m}$  region will improve mineral mapping. Similarly, mineral mapping might be improved where feasible by editing the MICA 2-micron command file to reduce the use of these longer wavelengths for RT-only data. Other significant wavelength regions affect a smaller number of minerals, specifically, the  $1.45$  to  $1.5 \mu\text{m}$  region, where a secondary absorption feature of alunite is found, and the  $1.75$  to  $1.8 \mu\text{m}$  region, where a secondary absorption feature of gypsum is located.

## 7. ACKNOWLEDGMENTS

Any use of trade, product, or firm names is for descriptive purposes only and does not imply endorsement by the U.S. Government. This work was funded by the U.S. Geological Survey Mineral Resources Program. We deeply appreciate the cooperation of the AVIRIS team at NASA/JPL in facilitating downloads of data and discussions regarding processing of AVIRIS data.

## 8. REFERENCES

- [1] Kokaly, R.F., King, T.V.V., and Hoefen, T.M., 2013, Surface mineral maps of Afghanistan derived from HyMap imaging spectrometer data, version 2: U.S. Geological Survey Data Series 787, 29 p.
- [2] Richter, R., and Schlapfer, D., 2019. Atmospheric/topographic correction for airborne imagery: ATCOR-4 User Guide Version 7.3.0. German Aerospace Center, DLR-IB 564-02.
- [3] Clark, R.N., Swayze, G.A., Livo, K.E., Kokaly, R.F., King, T.V., Dalton, J.B., Vance, J.S., Rockwell, B.W., Hoefen, T., and McDougal, R.R., 2002, Surface reflectance calibration of terrestrial imaging spectroscopy data: A tutorial using AVIRIS. In *Proc. 10th Airborne Earth Science Workshop*, JPL Publication 02-1, Pasadena, CA.
- [4] Graham, G.E., Kokaly, R.F., Kelley, K.D., Hoefen, T.M., Johnson, M.R., and Hubbard, B.E., 2018, Application of imaging spectroscopy for mineral exploration in Alaska: A study over porphyry Cu deposits in the eastern Alaska Range: *Economic Geology*, vol. 113, no. 2, pp. 489-510.